Liquid lubrication in sheet metal forming at mesoscopic scale

Hubert, C.; Dubar, L.; Bay, Niels; Christiansen, Peter; Dubois, A.

Published in:
Proceedings of the 7th ICFG Workshop on Process Simulation in Metalforming

Publication date:
2012

Proceedings of the 7th ICFG Workshop on Process Simulation in Metalforming
12-14 September, 2012, Gifu, Japan

Liquid lubrication mechanisms in sheet metal forming at mesoscopic scale

C. Hubert[1], L. Dubar[1*], P. Christiansen[2], N. Bay[2], A. Dubois[1]

[1] TEMPo EA 4542, University of Valenciennes and Hainaut Cambresis, France

[2] Department of Mechanical Engineering, Technical University of Denmark, Denmark

[*] laurent.dubar@univ-valenciennes.fr

Keywords: metal forming, fluid lubrication mechanisms, analysis on mesoscopic scale

Abstract. The lubricant entrapment and escape phenomena in metal forming are studied experimentally as well as numerically. Experiments are carried out in strip reduction of aluminium sheet applying a transparent die to study the fluid flow between mesoscopic cavities. The numerical strategy is based on a weak fluid/structure coupling involving the Finite Element Method and analytical calculations. It allows to quantify the final shape of the lubricant pockets

1. Introduction

Many metal forming operations involve liquid lubricants to reduce friction at the tool/part interface and to improve the finished part surface quality. In most of these operations the mixed lubrication regime appears, leading to local asperity contact between the tool and part surfaces in between pockets functioning as micro-reservoirs for the lubricant. During processing the reservoirs are deformed and the entrapped lubricant is pressurized and eventually escaping leading to local, non-uniform deformation of the surface layer. It is of great importance to understand and control the lubrication phenomena in order to reduce friction and improve the resulting surface quality. The present work involves numerical as well as experimental analyses of the lubrication mechanisms, applying the numerical strategy developed by Deltombe et al. [1] to quantify the final shape of the lubricant pockets, and the testing device involved in Bech et al. [2] work to calibrate the numerical model.

2. Numerical model for fluid exchange calculation

The numerical methodology developed in [1] involves a Finite Element (FE) fully coupled fluid-structure computation for its initialization, without lubricant exchange, followed by a computation loop including two calculation steps.

The first step is performed by an external subroutine computing the fluid flow between each lubricant reservoirs. The lubricant flow rates q_{ij} related to the i^{th} cavity in the FE model are calculated using a development of the local Couette's equation in terms of pressure gradient, supplied by the results of the initial (or previous) FEM computation:

$$q_{i1} = -\frac{h^3}{12\eta}\frac{\Delta p_{i1}}{\Delta x_{i1}} + u_1 h \quad \text{and} \quad q_{i2} = -\frac{h^3}{12\eta}\frac{\Delta p_{i2}}{\Delta x_{i2}} - u_2 h, \tag{1}$$

where h is the lubricant film thickness between the die and the asperity plateaus, η is the lubricant dynamic viscosity coefficient, Δp_{ij} is the pressure gradient between the current cavity and the previous cavity (if $j = 1$) or the subsequent cavity (if $j = 2$), u_j is the relative tool/plateau velocity and Δx_{ij} is the previous or subsequent plateau length, depending on j. The parameters detailed above are illustrated in Fig. 1. The flow rates q_{ij} are then summed to obtain the global flow rate $q_i = q_{i1} + q_{i2}$ related to each cavity, its sign indicating whether flow is into or out of the cavity.

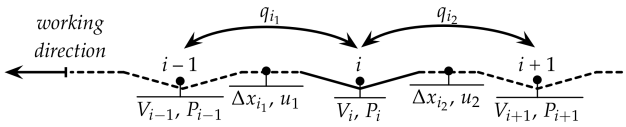

Fig. 1. Illustration of fluid exchange between lubricant pockets.

The calculated fluid rates are then applied as boundary conditions to a new fluid-structure FE computation, corresponding to the second step. The FE model involves both dies, modelled as rigid bodies, and the strip provided with cavities, modelled with 2D fluid link elements. The FE model is illustrated in Fig. 2 with its geometrical parameters. During the calculation the fluid interacts with the solid elements, leading to modifications of the fluid pressure owing to the plastic deformation of the strip. By the end of the calculation, the new pressure state is known for all the cavities, as well as the asperity plateau contact length and relative velocity between die and strip asperity plateaus.

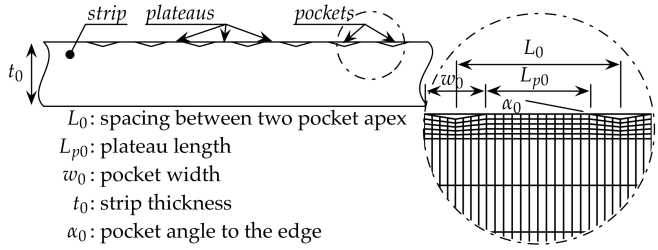

Fig. 2. Finite Element model configuration.

3. Experimental investigations

The experimental testing device used in this study is developed by Bech et al. [2] for thickness reduction of aluminium strips provided with cavities filled with lubricant. Using an upper die of hardened glass direct observation with a high speed video camera of lubricant entrapment and escape during drawing is enabled (Fig. 3a). The thickness reduction is ensured by an inclined lower steel die. The drawing speed V_s is adjustable. Mesoscopic pockets are manufactured on the upper strip surface to model the influence of micro-pockets appearing in a real surface. These pockets are in shape of triangular grooves (Fig. 3b) to ensure plane strain behaviour of the lubricant. The strip dimensions are $l_0 \times b_0 \times t_0 = 450 \times 20 \times 2\text{mm}$, and its material is a AISI 1050 H24 aluminium. In the present study the pocket angle to the edge is $\alpha_0 = 5°$.

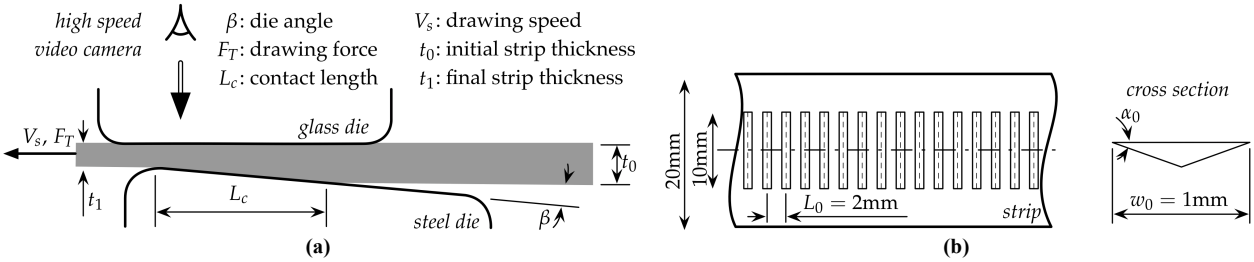

Fig. 3. Schema of the experimental testing device **(a)** and groove pattern on the specimens **(b)**.

Test conditions involve two drawing velocities $V_{s1} = 5\text{mm.s}^{-1}$ and $V_{s2} = 50\text{mm.s}^{-1}$, and two lubricant viscosities $\eta_1 = 0.054\text{Pa.s}$ and $\eta_2 = 0.595\text{Pa.s}$. All parameters are crossed each others leading to four test configurations, with three tests per configuration. During the tests the drawing speed and force are recorded, the latter in order to calibrate friction in the FE model.

The dimensions given in Fig. 3b are target values that are difficult to respect, mainly because of electrode wear during the Electro-Discharge Machining of the grooves. The actual dimensions are given in Table 1 along with the final dimensions, after testing.

Table 1. Initial and final strip thickness and surface topography. Parameters defined in Fig. 2 and 3b.

Parameter	V_{s1},η_1	V_{s1},η_2	V_{s2},η_1	V_{s2},η_2
t_0 (mm)	1.96	1.96	1.96	1.96
t_1 (mm)	1.68	1.68	1.59	1.68
w_0 (mm)	1.34	1.36	1.44	0.97
L_{p0} (mm)	0.66	0.64	0.56	1.03
α_0	3.69°	4.99°	4.68°	3.73°
d_0 (μm)	39	51	54	25
d_1 (μm)	5	9	17	7

4. Experimental-Numerical comparison

4.1. Set-up of Finite Element models

Firstly, the geometry of the FE models related to each test configuration is adjusted to match the actual, experimental ones (Table 1). Secondly, friction in the contact between tool and workpiece must be determined. Coulomb's law is adopted and a global friction coefficient is identified for both contact surfaces since it turns out to have no significant influence on the calculated lubricant flow.

4.2. Determination of the lubricant film thickness

It is assumed that the average roughness R_a is a good estimate of the lubricant film thickness after forming [3]. It is measured on square plateau regions of dimension $0.5\times0.5\text{mm}^2$ and the roughness is determined along three lines, perpendicular to the drawing direction. They are given in Table 2 together with their lower and upper bounds, for each testing condition.

Table 2. Determined lubricant film thicknesses.

Test condition	V_{s1},η_1	V_{s1},η_2	V_{s2},η_1	V_{s2},η_2
Lower bound (μm)	0.417	0.060	0.221	0.234
Mean value (μm)	**0.509**	**0.132**	**0.300**	**0.747**
Upper bound (μm)	0.601	0.204	0.379	1.260

The roughness measurement is local and may be strongly modified depending on the lubricant flow as noticed by Bech et al. [2], who observed significant increase in roughness in regions where lubricant escape occurred. This explains the important differences observed when comparing the tests two by two. The video recordings in tests V_{s1},η_2 and V_{s2},η_1 that give the lowest roughness values in Table 2, show forward lubricant escape mainly from the grooves corners rather than from the front edge. It thus implies lower roughness value since the lubrication is probably closer to boundary lubrication rather than hydrodynamic. On the contrary tests V_{s1},η_1 and V_{s2},η_2 with lubricant escape to the plateau result in surface roughening indicating hydrodynamic lubrication (the initial strip roughness was $R_{a0} = 0.463\mu\text{m}$).

4.3. Experimental and numerical depth of final pocket

The 2D FE model leaves the pocket depth as the most relevant characteristic when validating the model by comparisons with experiments. The numerical model allows monitoring of the pocket evolution when passing through the deformation zone, and comparison with the experiments is achieved in terms of final depth. For each test condition, the computation is given for the mean h value as well as for the lower and upper bound of the film thickness h shown in Table 2, indicating the large scatter of this parameter and the difficulties to determine a representative value.

Fig. 6a shows the results for test V_{s1},η_1. The read curve represents the cavity depth development predicted on basis of the mean film thickness, whereas the read shaded area shows the variation in predicted cavity depth within the film thickness range listed in Table 2. A strong decrease in pocket depth is noticed at the entrance before the cavity is fully covered by the glass die. It corresponds to a significant lubricant escape caused by the pressure gradient related to the

considered cavity towards the neighbouring inlet zone with atmospheric pressure. Once the cavity is fully closed, the cavity depth evolution is much less pronounced but varying in a non-monotonic way owing to other cavities entering and exiting the contact zone. At the end of the contact, the pressure gradient of the pocket is again computed against atmospheric pressure, leading to fluid loss from the cavity to the exit implying a cavity depth reduction.

Fig. 6a shows that the mean h allows good prediction of the final cavity depth, but the depth prediction is very sensitive to the lubricant film thickness adopted. The figure shows a final depth corridor range of $0 \leq d_1 \leq 23\mu$m.

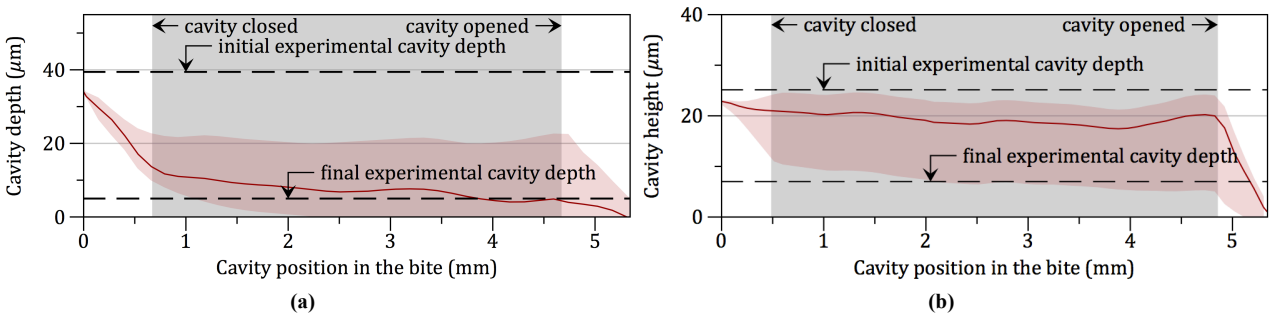

Fig. 6. Numerical and experimental cavities depth for conditions V_{s1}, η_1 **(a)** and V_{s2}, η_2 **(b)**.

In test V_{s2}, η_2 (Fig. 6b) the same observation is made as in test V_{s1}, η_1 concerning the sensitivity of the lubricant film thickness, which is explained by the wide film thickness range observed in this case (Table 2). With this range the calculated final cavity depth lies in the range $5 \leq d_1 \leq 24\mu$m, while the final experimental cavity depth is $d_1 = 7\mu$m. The one predicted for the mean film thickness is $d_1 = 20\mu$m. The results highlight the importance of determining the film thickness accurately. This is emphasized by the fact that h is raised to the power of 3 in the Couette equation (1) implying decisive influence on the lubricant flow rate.

The predicted cavity depths for conditions V_{s1}, η_2 and V_{s2}, η_1 are completely different from V_{s1}, η_1 and V_{s2}, η_2. As explained in Section 4.2 escape of lubricant in these two tests mainly occurred from the groove corners resulting in less lubricant on the plateaus and thus in small film thickness h. Since the model does not take this alternative lubricant flow into account it fails to predict the experimentally observed cavity depth reduction.

5. Conclusions

The model clearly identifies the lubricant film thickness as a key parameter, which is difficult to determine. Further investigations may be carried out to get statistically based film thicknesses rather than deterministic values which among others are heavily influenced by the measurement location. The model is not able to predict consistent cavities depth reduction for two tests cases, where the visual observations showed lubricant escape to be highly inhomogeneous occurring from the corner points. This is, however, considered to be an experimental rather than a numerical error.

References

[1] R. Deltombe, A. Belotserkovets, M. Dubar, A. Dubois, L. Dubar, Proceedings of the Institute of Mechanical Engineers Part J – J. Eng. Trib. 225/9, 887–893 (2011).

[2] J. Bech, N. Bay, M. Eriksen, Wear, 232, 134–139 (1999).

[3] N. Bay, T. Wanheim, Proceedings of the 3rd ICTP conference, 1677–1691 (1990).